





Huge linear magnetoresistance due to open orbits in  $\gamma$ -PtBi<sub>2</sub>Beilun Wu <sup>1</sup>, Víctor Barrena <sup>1</sup>, Hermann Suderow <sup>1,2</sup> and Isabel Guillamón <sup>1,2,\*</sup><sup>1</sup>Laboratorio de Bajas Temperaturas y Altos Campos Magnéticos, Departamento de Física de la Materia Condensada, Instituto Nicolás Cabrera and Condensed Matter Physics Center (IFIMAC), Universidad Autónoma de Madrid, E-28049 Madrid, Spain<sup>2</sup>Unidad Asociada de Bajas Temperaturas y Altos Campos Magnéticos, UAM, CSIC, Cantoblanco, E-28049 Madrid, Spain

(Received 22 January 2020; accepted 20 April 2020; published 18 May 2020)

Some single-crystalline materials present an electrical resistivity which decreases between room temperature and low temperatures at zero magnetic field as in a good metal and switches to a nearly semiconductinglike behavior at low temperatures with the application of a magnetic field. Often, this is accompanied by a huge and nonsaturating linear magnetoresistance which remains difficult to explain. Here, we present a systematic study of the magnetoresistance in single-crystal  $\gamma$ -PtBi<sub>2</sub>. We observe that the angle between the magnetic field and the crystalline  $c$  axis fundamentally changes the magnetoresistance, going from a saturating to a nonsaturating magnetic-field dependence. In between, there is one specific angle where the magnetoresistance is perfectly linear with the magnetic field. We show that the linear dependence of the nonsaturating magnetoresistance is due to the formation of open orbits in the Fermi surface of  $\gamma$ -PtBi<sub>2</sub>.

DOI: [10.1103/PhysRevResearch.2.022042](https://doi.org/10.1103/PhysRevResearch.2.022042)

Magnetoresistance (MR) is the modification of the electrical resistance by a magnetic field. MR is a ubiquitous phenomenon in metals and semiconductors, although it is not expected to occur just considering free electrons without interactions. The electrical resistivity  $\rho$  occurs due to scattering of electrons on a timescale  $\tau$ , and the main consequence of applying a magnetic field is spiraling the electron orbits with an angular velocity  $\omega_c = \frac{eB}{m^*}$  (with  $e$  as the electron charge and  $m^*$  as the electronic effective mass). When considering nearly free electrons, the simplest magnetic-field dependence found for the magnetoresistance is quadratic  $\rho(B) \propto B^2$ , obeying Onsager's reciprocity condition  $\rho(B) = \rho(-B)$ . Furthermore, the MR saturates in the high-field limit ( $\omega_c \tau \gg 1$ ) unless electron and hole numbers are close to compensate with each other in which case, it continues growing as  $\rho(B) \propto B^2$ . In metals with no or weak electronic correlations, a small quadratic MR saturating at high fields is, indeed, often observed [1–3], with a few exceptions, such as the semimetal Bi and other electron-hole compensated metals [4–7]. More intriguing and difficult to explain is the observation of a huge and nonsaturating linear magnetoresistance, which has been recently discussed in a number of materials. The magnetoresistance is also influenced by contributions from open orbits, which play sometimes a role, often leading to a sizable enhancement, which was, however, not considered as sufficient to explain huge magnetoresistances [1–3]. Here, we show that the direction of the magnetic field produces an unanticipated huge enhancement

of the linear magnetoresistance exactly when the contribution of open orbits to the magnetoresistance is maximal.

There are a number of metallic or semimetallic compounds showing large and sometimes linear magnetoresistances [7–22]. The semimetal  $\gamma$ -PtBi<sub>2</sub> stands out among these compounds because of the extreme values of the magnetoresistance [23].  $\gamma$ -PtBi<sub>2</sub> has a layered structure with trigonal symmetry [space-group  $P31m$ , No. 157, see Fig. 1(a)]. Electronic band-structure calculations [23,24] show that this compound has a Fermi surface containing multiple electron and hole sheets. Angle-resolved photoemission spectroscopy (ARPES) [25,26] and quantum oscillation studies [23] have measured the band structure and the Fermi surface. In particular, the ARPES data [26] revealed a spin-polarized surface state with linear dispersion, which was associated with the linear MR reported in an early study [27].

Here, we make detailed measurements of the angular-dependent MR up to 22 T on a high quality single crystal of  $\gamma$ -PtBi<sub>2</sub>. To analyze effects only due to the crystalline orientation to the magnetic field, we keep the field direction perpendicular to the electrical current. We observe a continuous evolution from a saturating sublinear MR for  $\mathbf{B} \parallel \mathbf{c}$  to a nonsaturating quadraticlike MR for the field on the plane. The linear nonsaturating MR is only observed for a specific angle of the magnetic field with respect to the  $c$  axis. We show that such a linear MR appears at a specific angle in the presence of open orbits.

We grew single crystals of  $\gamma$ -PtBi<sub>2</sub> [28] using the Bi self-flux method described in Ref. [23]. We used the equipment described in Ref. [29], in particular, frit crucibles [30]. Powder x-ray diffraction of our crystals reveals the expected crystal structure [Fig. 1(b)] together with some peaks corresponding to residual Bi flux and Bi oxides. We measured a neat  $\gamma$ -PtBi<sub>2</sub> single-crystal platelet, oriented with the  $c$  axis out of the plane [inset of Fig. 1(b)]. The residual resistance ratio is of 100, showing excellent sample quality. To measure the MR,

\*Corresponding author: [isabel.guillamon@uam.es](mailto:isabel.guillamon@uam.es)

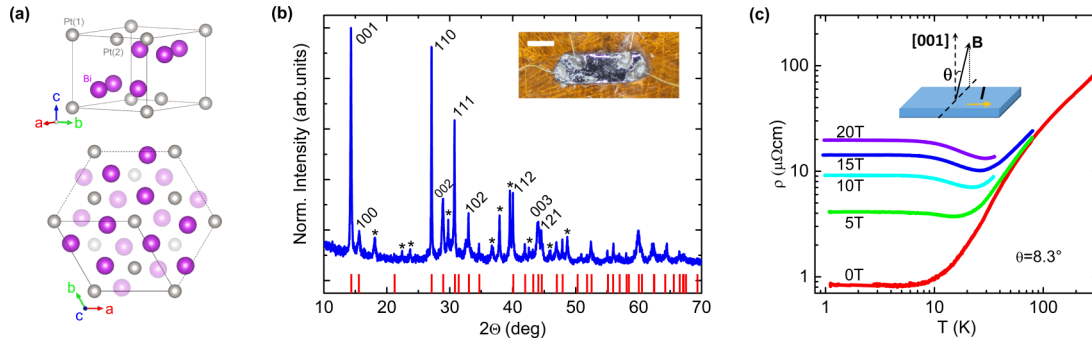


FIG. 1. (a) Crystal structure of the layered  $\gamma$ -PtBi<sub>2</sub>. (b) In blue, we show the x-ray diffraction pattern of  $\gamma$ -PtBi<sub>2</sub> powder. Red bars show the positions of the peaks expected to appear in this compound. The asterisks mark the peaks associated with residual Bi and Bi oxides from flux growth. The inset shows a picture of the single crystal with four contacts used for resistivity measurements. The white scale bar is 0.2-mm long. (c) Colored lines show the temperature dependence of the resistivity at different magnetic fields. The field is applied at an angle  $\theta = 8.3^\circ$ , which is also the precise angle at which we find nonsaturating linear magnetoresistance. The temperature dependence is very similar for all field orientations. The inset shows a scheme of the direction of the applied current and magnetic field.

we used a cryostat capable of reaching about 1 K [31], and a (20 + 2) T superconducting magnet supplied by Oxford Instruments [32]. We used a homemade mechanical rotator, described in the Supplemental Material [33], to modify the field angle. The current was applied perpendicular to the magnetic field [inset in Fig. 1(c)]. The rotator allowed an angular range covering from the field along the  $c$  axis ( $\theta = 0^\circ$ ) to parallel to the plane ( $\theta = 90^\circ$ ). The angle of the magnetic field was measured using a Hall probe [34]. We define  $MR = \frac{\rho(B) - \rho(0)}{\rho(0)}$  with  $\rho(0)$  being the resistivity at zero magnetic field and provide it in percentages. To find Shubnikov–de Haas oscillations, we obtain the oscillatory component  $\Delta MR$  by fitting the MR data above 13 T to a low-order polynomial and perform the Fourier transform of  $\Delta MR(1/B)$ .

Figure 1(c) shows the resistivity as a function of temperature at different magnetic fields. We find a metallic behavior at zero field and a semiconductinglike behavior under magnetic fields (resistivity increases with decreasing temperature at low temperatures). The semiconductinglike increase saturates below about 8 K.

Figure 2 shows the transverse MR up to 20 T for different orientations of the magnetic field from  $\mathbf{B} \parallel c$  ( $\theta = 0^\circ$ ) to  $\mathbf{B} \perp c$  ( $\theta = 90^\circ$ ). The highest value of the MR is of 5800% at 20 T for  $\theta$  close to  $90^\circ$ . For magnetic fields below 5 T, we always find a quadratic MR. For higher fields, we observe an angular evolution of the MR from a concave curvature (saturating MR) at  $\theta = 0^\circ$  to a quadraticlike convex curvature (nonsaturating MR) at  $\theta$  close to  $90^\circ$ . The magnitude of the MR changes by a factor of 5 as a function of the angle at high magnetic fields. In between the concave and convex magnetic-field dependencies, we observe a perfectly linear MR at  $\theta = 8.3^\circ$ .

To see this, we fit the data above 5 T with an empirical power law  $MR(B) = c + aB^\alpha$ . We find an increasing  $\alpha$  with  $\theta$  (inset of Fig. 2) up to 1.65. At  $\theta = 8.3^\circ$ ,  $\alpha = 1$ , and the MR changes from saturating to nonsaturating behavior.

Figure 3(a) shows the quantum oscillation pattern in the MR for  $\theta = 8.3^\circ$  as a function of the magnetic field. Figures 3(b)–3(d) present the Fourier transform of the quantum oscillation signal as a function of  $\theta$ . Each quantum oscillation frequency  $F$  is related to an extremal cross-sectional area of the Fermi surface normal to the field  $\mathcal{A}_k$  through the Onsager

relation  $F = (\hbar/2\pi e)\mathcal{A}_k$ . In Fig. 3(e), we track the quantum oscillation frequencies as a function of the angle. At  $\theta$  close to  $0^\circ$ , our result exactly coincides with the result in Ref. [23] (taken along the same field direction). We can, thus, identify several frequencies,  $F_\beta = 388$ ,  $F_\gamma = 1225$ , and  $F_\eta = 3012$  T using the same notation [23]. The results for finite  $\theta$  are new, and we use the same notation extrapolating from  $\theta = 0^\circ$ . We measure in a smaller field range than Ref. [23]. As a result, two low-frequency orbits (at 40 and at 15 T) are not well defined in our data. On the other hand, we can sweep the magnetic field much more slowly and, thus, resolve better the high-frequency quantum oscillations. For instance, we observe a high-frequency oscillation around  $F_\tau = 4440$  T. The

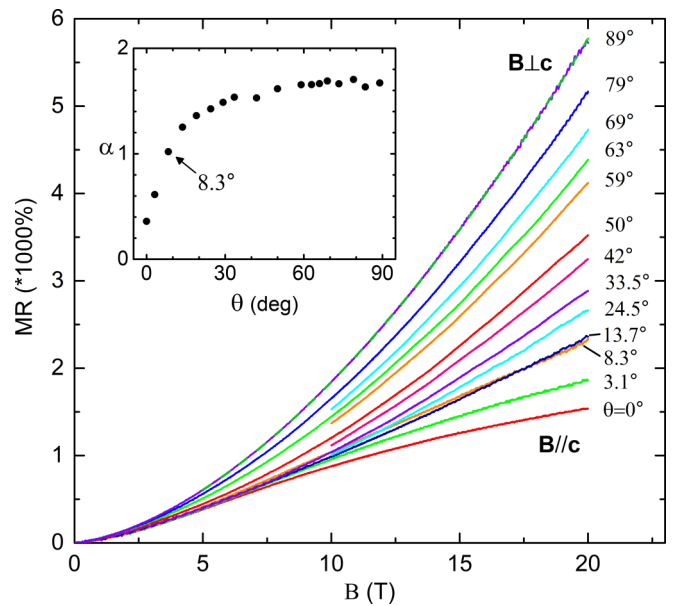


FIG. 2. MR up to 20 T for different field directions from  $\mathbf{B} \parallel c$  ( $\theta = 0^\circ$ ) to  $\mathbf{B} \perp c$  ( $\theta$  close to  $90^\circ$ ). The inset shows the angular dependence of the exponent  $\alpha$  obtained by fitting the MR at each angle with an empirical power law  $MR = c + aB^\alpha$ . The green broken line in the main figure shows, as an example, the fit for the data at  $\theta = 89^\circ$ .

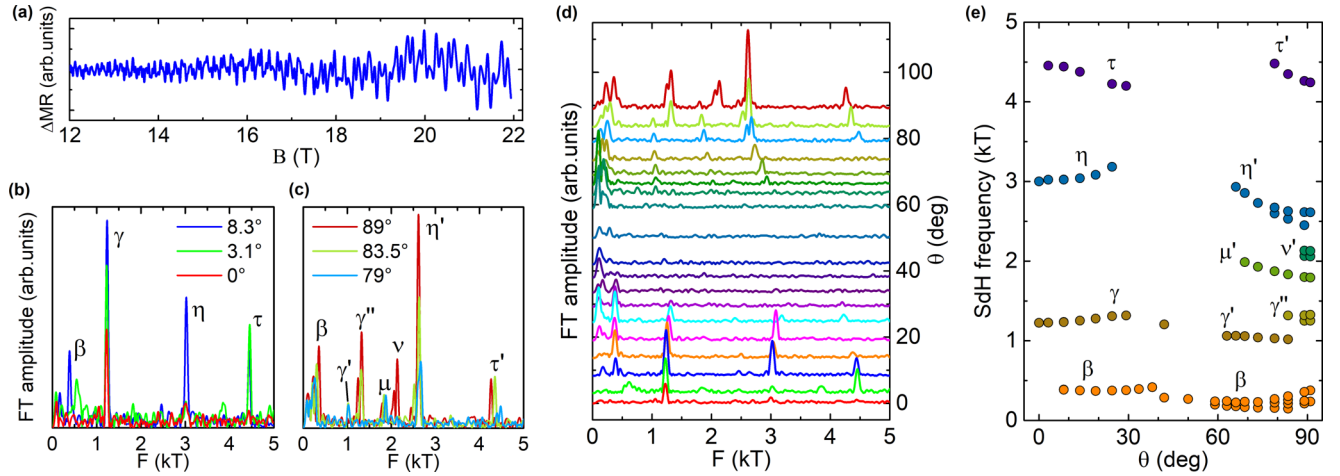


FIG. 3. (a)  $\Delta\text{MR}$  (defined in the text) versus magnetic field up to 22 T at  $T = 1$  K and  $\theta = 8.3^\circ$ . (b) and (c) Fourier transform of  $\Delta\text{MR}$  for a few values of  $\theta$ . Greek letters mark the oscillation frequencies giving peaks in the Fourier transforms. (d) Fourier transform of  $\Delta\text{MR}$  as a function of the frequency  $F$  for different  $\theta$ 's. Data are shifted along the y axis for clarity, following the value of  $\theta$ . (e) Angular evolution of the quantum oscillations frequencies with the corresponding orbits labeled by greek letters.

quantum oscillation pattern is very weak between  $\theta = 30^\circ$  and  $60^\circ$ , so we cannot resolve the frequency of the orbits in this angular range except for the orbit with the lowest-frequency  $\beta$ . We, thus, keep the notation for the orbits at  $\theta$  close to  $90^\circ$  as for similar frequencies at  $\theta$  close to  $0^\circ$  but add apostrophes. There are two extra frequencies that do not have direct counterparts at  $\theta$  close to  $0^\circ$ , and we denote them as  $F_{\mu'} = 1798$  and  $F_{\nu'} = 1798$  T. Furthermore, we observe that  $\eta'$ ,  $\gamma''$ , and  $\nu'$  split into two and  $\beta$  into three frequencies close to  $90^\circ$ .

We have also measured the temperature dependence of the quantum oscillations at two different angles  $\theta = 8.3^\circ$  and  $\theta = 89^\circ$  where the oscillation amplitudes are the largest to obtain the quasiparticle effective mass  $m_i^*$  of each orbit and their quantum lifetime  $\tau_Q$  [see Figs. S1(a)–S1(c) and Table S1 in the Supplemental Material [33]).  $m_i^*$  lies close to the free-electron mass  $m_e$  for all the orbits except  $\beta$ , whereas the estimated  $\tau_Q$  ranges from 0.15 to 0.75 ps. We also analyze the phase of the lowest-frequency mode ( $\beta$ ) and obtain, for this orbit, a nontrivial Berry phase  $\Phi_B$  close to  $\pi$ . This result is in agreement with previous quantum oscillation measurements and suggests that the predicted triply degenerate point in the associated  $\beta$  band is likely to be present [23].

Band-structure calculations in  $\gamma$ -PtBi<sub>2</sub> [23,35] show many bands that cross the Fermi level, forming six or seven sheets. Spin-orbit coupling leads to large band splittings, and the shape of the Fermi-surface pockets is very sensitive to the position of the Fermi level. At the Fermi level, the bands have mixed electron-hole character with a somewhat larger density of holes [25,26]. We see that the smallest  $k_F$  ( $\beta$  orbit) in our quantum oscillation data is about 1/4 of the size of the first Brillouin zone and appears in pockets centered at the corners of the Brillouin zone derived from the  $\beta$  band [23]. The two high-frequency orbits ( $\eta$  and  $\tau$ ) are associated with the two bands producing large pancakelike Fermi-surface sheets centered at the top and the bottom of the Brillouin zone [23]. This particular shape gives extremal orbits only when  $\mathbf{B} \parallel \mathbf{c}$  or  $\perp \mathbf{c}$ , which explains the absence of corresponding frequencies at intermediate angles. We also find several orbits split into

two or more frequencies at  $\theta$  close to  $90^\circ$ . This probably comes from the warping of the corresponding Fermi-surface sheets [36].

The calculations in Ref. [23] reveal a  $\gamma$  band that has spherical-like Fermi-surface pockets arranged in a honeycomb lattice located on the plane and interconnected with each other through tilted necks. The lower inset of Fig. 4 presents schematically this open Fermi-surface sheet. We mark, by the red dashed lines, two planes perpendicular to a magnetic field tilted from the  $\mathbf{c}$  axis. These contain open orbits. In each of the planes, the spheres located at one side of the honeycomb structure are connected to each other but not with the spheres of the other side (upper left insets of Fig. 4). Electrons on open orbits go into noncircular trajectories, instead of following cyclotron motion [1,37]. This has a strong impact on the MR [1,37–39]. In a metal with a single electronic band, open orbits lead to a quadratic enhancement of the MR at certain field angles, leaving a usual saturated MR at the angles where the open orbits are absent [40,41]. Multiple Fermi-surface sheets as in  $\gamma$ -PtBi<sub>2</sub> are considered in detail here. To set up a MR model taking into account multiple sheets, we first consider that, in a semimetal, the MR has a  $B^2$  unsaturated behavior when the electron and hole numbers ( $n_e$  and  $n_h$ ) are compensated [1,7,42]. We consider a two-band model and take electrons as free carriers with the same mobility  $\mu$ . The level of electron-hole compensation is given by  $d = (n_e - n_h)/(n_e + n_h)$ . We add a field-independent small contribution from the open orbits  $\delta\sigma_0$  to the total conductivity  $\sigma_0$ . More details are provided in the Supplemental Material [33]. We can then write for the resistivity  $\rho(B)/\rho_0 = \frac{\delta(1+\eta^2)^2 + (1+\eta^2)}{\delta(1+\eta^2) + 1 + d^2\eta^2}$ , where  $\eta = \mu B$ .

We find that this reproduces nicely the linear MR at  $8.3^\circ$  (Fig. 4) and at all other field orientations (see Fig. S2 in the Supplemental Material [33]). We use, for this angle, the parameters  $\delta = 0.00849$ ,  $\mu = 4630 \text{ cm}^2 \text{ V}^{-1} \text{ s}^{-1}$  and  $|d| = 0.229$ . The size of  $\delta$  is small compared to one, in agreement with the fact that only a tiny proportion of the whole Fermi surface would be engaged in forming open orbits. From the mobility  $\mu$ , we estimate the transport mean free

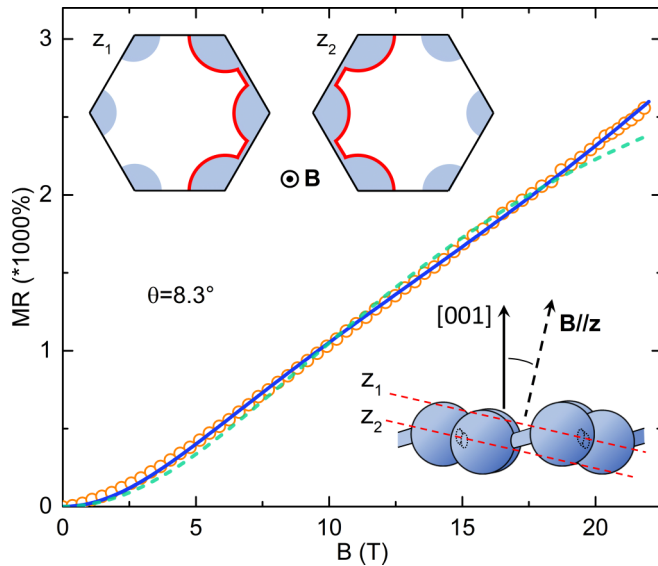


FIG. 4. We show, as orange circles, the MR at  $\theta = 8.3^\circ$  up to 22 T. By the blue line, we show the result of the model discussed in the text. The green dashed line shows the result of the same model but without contribution from open orbits. Note the saturation observed at high magnetic fields. In the lower right inset, we show schematically the  $\gamma$ -band Fermi-surface sheet. The shape is that of an undulated grid of spheres arranged in a honeycomb lattice perpendicular to the  $c$  axis [23]. The sheets are connected by necks oriented at an angle to the plane. Necks that lie behind the spheres are schematically represented by dashed lines. When the magnetic-field direction is slightly tilted from  $c$ , open orbits may appear on two different planes (marked by red dashed lines). The corresponding open orbits are provided in the upper left panels.

scattering time  $\tau_{tr}$  ( $\mu = e\tau_{tr}/m^*$ ) to be around  $2.6 \times 10^{-12}$  s, a few times larger than the quantum lifetime  $\tau_Q$  deduced from the amplitude of the quantum oscillations (Table S1 in the Supplemental Material [33]). This difference is reasonable as  $\tau_Q$  measures the smearing of the Landau levels due to forward and backward scatterings, whereas transport  $\tau_{tr}$  requires backscattering. The linear MR cannot be obtained without taking into account the open orbits ( $\delta$  term), and the MR would show a clear saturation at high fields due to an inexact compensation between the electron and the hole carrier numbers. It is, thus, the combination of both effects that leads to the observed linear MR at  $\theta = 8.3^\circ$ . For the other angles, we can associate the increase in the MR from  $0^\circ$  to

$90^\circ$  and the evolution of its curvature to changes in  $|d|$ , which steadily decreases from 0.22 at  $0^\circ$  to close to 0 at  $90^\circ$ .

The relevant contribution of a one-dimensional conduction channel for the magnetoresistance which we unveil here can have consequences, particularly, for the behavior at even larger magnetic fields. The Lebed effect consists of resonances occurring in open orbits for in- and out-of-plane transport between layers of a two-dimensional crystalline structure [43]. As a consequence, different kinds of oscillatory behavior related to open orbits have been predicted and observed in organic systems, including magic angles related to dimensional crossovers, strong angular-dependent oscillations, or density waves [44–47]. Our result suggests that such one-dimensional features could arise in semimetals due to open orbits.

This seems particularly interesting in view of the unconventional band structures often observed in semimetals. For  $\gamma$ -PtBi<sub>2</sub>, band-structure calculations suggest triply degenerate nodal points [20,21,23,26]. Contrary to Dirac and Weyl fermions [23,35,48,49], triple points have no counterpart in high-energy physics [35,48–50]. These could influence the magnetoresistance in the case of complex conduction paths involving open orbits induced by the magnetic field.

To summarize, we synthesized high quality single crystals of  $\gamma$ -PtBi<sub>2</sub> and measured the angular dependence of the MR up to 22 T. We reveal that, in addition to the known electron-hole compensation, open orbits produce an important modification of the transport under magnetic fields leading to huge values of the magnetoresistance and a linear field dependence. Additionally, we suggest that phenomena inherent to one-dimensional conduction might appear at ultrahigh magnetic fields in low carrier density semimetals.

This work was supported by the European Research Council PNICTEYES Grant Agreement No. 679080, by the Spanish Research State Agency (Grants No. FIS2017-84330-R, No. CEX2018-000805-M, and No. RYC-2014-15093) and by the Comunidad de Madrid through Program NANOMAGCOST-CM (Program No. S2018/NMT-4321). We acknowledge collaborations through the EU program Cost CA16218 (Nanocohybr). We particularly acknowledge SEGAINVEX at UAM for design and construction of cryogenic equipment. We also thank R. Álvarez Montoya and J. M. Castilla for technical support and S. Delgado for support with the single-crystal growth. We learned of the search for new materials with P. C. Canfield and are very grateful to him for this. We acknowledge SIDI at UAM for support in sample characterization.

- [1] A. Pippard, *Magnetoresistance in Metals*, Cambridge Studies in Low Temperature Physics (Cambridge University Press, Cambridge, UK, 1989).
- [2] A. Abrikosov, *Fundamentals of the Theory of Metals* (Dover, New York, 2017).
- [3] P. Kapitza, The change of electrical conductivity in strong magnetic fields. Part I.—Experimental results, *Proc. R. Soc. London, Ser. A* **123**, 292 (1929).

- [4] Z. Zhu, B. Fauqué, K. Behnia, and Y. Fuseya, Magnetoresistance and valley degree of freedom in bulk bismuth, *J. Phys.: Condens. Matter* **30**, 313001 (2018).
- [5] P. B. Alers and R. T. Webber, The magnetoresistance of bismuth crystals at low temperatures, *Phys. Rev.* **91**, 1060 (1953).
- [6] F. Y. Yang, K. Liu, C. L. Chien, and P. C. Searson, Large Magnetoresistance and Finite-Size Effects in Electrodeposited Single-Crystal Bi Thin Films, *Phys. Rev. Lett.* **82**, 3328 (1999).

- [7] M. N. Ali, J. Xiong, S. Flynn, J. Tao, Q. D. Gibson, L. M. Schoop, T. Liang, N. Haldolaarachchige, M. Hirschberger, N. P. Ong, and R. J. Cava, Large, non-saturating magnetoresistance in  $\text{WTe}_2$ , *Nature (London)* **514**, 205 (2014).
- [8] F. F. Tafti, Q. D. Gibson, S. K. Kushwaha, N. Haldolaarachchige, and R. J. Cava, Resistivity plateau and extreme magnetoresistance in  $\text{LaSb}$ , *Nat. Phys.* **12**, 272 (2015).
- [9] Y. Feng, Y. Wang, D. M. Silevitch, J.-Q. Yan, R. Kobayashi, M. Hedo, T. Nakama, Y. Onuki, A. V. Suslov, B. Mihaila, P. B. Littlewood, and T. F. Rosenbaum, Linear magnetoresistance in the low-field limit in density-wave materials, *Proc. Natl. Acad. Sci. USA* **116**, 11201 (2019).
- [10] I. A. Leahy, Y.-P. Lin, P. E. Siegfried, A. C. Treglia, J. C. W. Song, R. M. Nandkishore, and M. Lee, Nonsaturating large magnetoresistance in semimetals, *Proc. Natl. Acad. Sci. U.S.A.* **115**, 10570 (2018).
- [11] S. Mitra, J. G. S. Kang, J. Shin, J. Q. Ng, S. S. Sunku, T. Kong, P. C. Canfield, B. S. Shastry, P. Sengupta, and C. Panagopoulos, Quadratic to linear magnetoresistance tuning in  $\text{TmB}_4$ , *Phys. Rev. B* **99**, 045119 (2019).
- [12] S. L. Bud'ko, P. C. Canfield, C. H. Mielke, and A. H. Lacerda, Anisotropic magnetic properties of light rare-earth dantimonides, *Phys. Rev. B* **57**, 13624 (1998).
- [13] K. Myers, S. Bud'ko, I. Fisher, Z. Islam, H. Kleinke, A. Lacerda, and P. Canfield, Systematic study of anisotropic transport and magnetic properties of  $\text{RAgSb}_2$  ( $\text{R}=\text{Y}, \text{La-Nd}, \text{Sm}, \text{Gd-Tm}$ ), *J. Magn. Magn. Mater.* **205**, 27 (1999).
- [14] E. Mun, H. Ko, G. J. Miller, G. D. Samolyuk, S. L. Bud'ko, and P. C. Canfield, Magnetic field effects on transport properties of  $\text{PtSn}_4$ , *Phys. Rev. B* **85**, 035135 (2012).
- [15] Y. Wu, L.-L. Wang, E. Mun, D. D. Johnson, D. Mou, L. Huang, Y. Lee, S. L. Bud'ko, P. C. Canfield, and A. Kaminski, Dirac node arcs in  $\text{PtSn}_4$ , *Nat. Phys.* **12**, 667 (2016).
- [16] R. F. Luccas, A. Fente, J. Hanko, A. Correa-Orellana, E. Herrera, E. Climent-Pascual, J. Azpeitia, T. Pérez-Castañeda, M. R. Osorio, E. Salas-Colera, N. M. Nemes, F. J. Mompean, M. García-Hernández, J. G. Rodrigo, M. A. Ramos, I. Guillaumon, S. Vieira, and H. Suderow, Charge density wave in layered  $\text{La}_{1-x}\text{Ce}_x\text{Sb}_2$ , *Phys. Rev. B* **92**, 235153 (2015).
- [17] J. A. Galvis, H. Suderow, S. Vieira, S. L. Bud'ko, and P. C. Canfield, Scanning tunneling microscopy in the superconductor  $\text{LaSb}_2$ , *Phys. Rev. B* **87**, 214504 (2013).
- [18] H.-Y. Yang, T. Nummy, H. Li, S. Jaszewski, M. Abramchuk, D. S. Dessau, and F. Tafti, Extreme magnetoresistance in the topologically trivial lanthanum mononictide  $\text{LaAs}$ , *Phys. Rev. B* **96**, 235128 (2017).
- [19] C. Shekhar, A. K. Nayak, Y. Sun, M. Schmidt, M. Nicklas, I. Leermakers, U. Zeitler, Y. Skourski, J. Wosnitza, Z. Liu, Y. Chen, W. Schnelle, H. Borrmann, Y. Grin, C. Felser, and B. Yan, Extremely large magnetoresistance and ultrahigh mobility in the topological Weyl semimetal candidate  $\text{NbP}$ , *Nat. Phys.* **11**, 645 (2015).
- [20] B. Q. Lv, Z.-L. Feng, Q.-N. Xu, X. Gao, J.-Z. Ma, L.-Y. Kong, P. Richard, Y.-B. Huang, V. N. Strocov, C. Fang, H.-M. Weng, Y.-G. Shi, T. Qian, and H. Ding, Observation of three-component fermions in the topological semimetal molybdenum phosphide, *Nature (London)* **546**, 627 (2017).
- [21] J.-Z. Ma, J.-B. He, Y.-F. Xu, B. Q. Lv, D. Chen, W.-L. Zhu, S. Zhang, L.-Y. Kong, X. Gao, L.-Y. Rong, Y.-B. Huang, P. Richard, C.-Y. Xi, E. S. Choi, Y. Shao, Y.-L. Wang, H.-J. Gao, X. Dai, C. Fang, H.-M. Weng, G.-F. Chen, T. Qian, and H. Ding, Three-component fermions with surface Fermi arcs in tungsten carbide, *Nat. Phys.* **14**, 349 (2018).
- [22] N. H. Jo, Y. Wu, L.-L. Wang, P. P. Orth, S. S. Downing, S. Manni, D. Mou, D. D. Johnson, A. Kaminski, S. L. Bud'ko, and P. C. Canfield, Extremely large magnetoresistance and Kohler's rule in  $\text{PdSn}_4$ : A complete study of thermodynamic, transport, and band-structure properties, *Phys. Rev. B* **96**, 165145 (2017).
- [23] W. Gao, X. Zhu, F. Zheng, M. Wu, J. Zhang, C. Xi, P. Zhang, Y. Zhang, N. Hao, W. Ning, and M. Tian, A possible candidate for triply degenerate point fermions in trigonal layered  $\text{PtBi}_2$ , *Nat. Commun.* **9**, 3249 (2018).
- [24] C. Q. Xu, X. Z. Xing, X. Xu, B. Li, B. Chen, L. Q. Che, X. Lu, J. Dai, and Z. X. Shi, Synthesis, physical properties, and band structure of the layered bismuthide  $\text{PtBi}_2$ , *Phys. Rev. B* **94**, 165119 (2016).
- [25] Q. Yao, Y. P. Du, X. J. Yang, Y. Zheng, D. F. Xu, X. H. Niu, X. P. Shen, H. F. Yang, P. Dudin, T. K. Kim, M. Hoesch, I. Vobornik, Z.-A. Xu, X. G. Wan, D. L. Feng, and D. W. Shen, Bulk and surface electronic structure of hexagonal structured  $\text{PtBi}_2$  studied by angle-resolved photoemission spectroscopy, *Phys. Rev. B* **94**, 235140 (2016).
- [26] S. Thirupathaiah, Y. Kushnirenko, E. Haubold, A. V. Fedorov, E. D. L. Rienks, T. K. Kim, A. N. Yaresko, C. G. F. Blum, S. Aswartham, B. Büchner, and S. V. Borisenko, Possible origin of linear magnetoresistance: Observation of Dirac surface states in layered  $\text{PtBi}_2$ , *Phys. Rev. B* **97**, 035133 (2018).
- [27] X. Yang, H. Bai, Z. Wang, Y. Li, Q. Chen, J. Chen, Y. Li, C. Feng, Y. Zheng, and Z.-a. Xu, Giant linear magnetoresistance in nonmagnetic  $\text{PtBi}_2$ , *Appl. Phys. Lett.* **108**, 252401 (2016).
- [28] N. Zhuravlev and L. Kertes, Structure of superconductors. XI. Investigation of alloys of bismuth with platinum, ruthenium, osmium and iridium, *JETP* **5**, 1073 (1957).
- [29] P. C. Canfield and Z. Fisk, Growth of single crystals from metallic fluxes, *Philos. Mag.* **B 65**, 1117 (1992).
- [30] P. C. Canfield, T. Kong, U. S. Kaluarachchi, and N. H. Jo, Use of frit-disc crucibles for routine and exploratory solution growth of single crystalline samples, *Philos. Mag.* **96**, 84 (2016).
- [31] R. A. Montoya, S. Delgado, J. Castilla, J. Navarrete, N. D. Contreras, J. R. Marijuan, V. Barrena, I. Guillaumon, and H. Suderow, Methods to simplify cooling of liquid helium cryostats, *HardwareX* **5**, e00058 (2019).
- [32] Commissioning note by Oxford Instruments, <https://www.oxinst.com/news/oxford-instruments-commissions-22-tesla-superconducting-magnet-system/>.
- [33] See Supplemental Material at <http://link.aps.org/supplemental/10.1103/PhysRevResearch.2.022042> for (i) details of the analyses of the Shubnikov-de Haas quantum oscillations, (ii) a detailed semiclassical model taking into account the open orbits to explain the magnetoresistance in the whole angular range, (iii) angular dependence of the magnetoresistance, and (iv) description of the mechanical rotator setup for resistivity measurements.
- [34] Hall probes from Arepok, <http://www.arepok.sk/?p=home>.
- [35] H. Weng, C. Fang, Z. Fang, and X. Dai, Coexistence of Weyl fermion and massless triply degenerate nodal points, *Phys. Rev. B* **94**, 165201 (2016).

- [36] A. Carrington, J. D. Fletcher, and H. Harima, Interpretation of the angular dependence of the de Haas-van Alphen effect in  $\text{MgB}_2$ , *Phys. Rev. B* **71**, 174505 (2005).
- [37] I. Lifshitz, M. I. Azbel, and M. Kaganov, The theory of galvanomagnetic effects in metals, *JETP* **4**, 41 (1957).
- [38] I. Lifshitz and V. G. Peschanskii, Galvanomagnetic characteristics of metals with open Fermi surfaces. I, *JETP* **8**, 875 (1959).
- [39] I. Lifshitz and V. G. Peschanskii, Galvanomagnetic characteristics of metals with open Fermi surfaces. II, *JETP* **11**, 137 (1960).
- [40] J. R. Klauder, W. A. Reed, G. F. Brennert, and J. E. Kunzler, Study of the fine structure in the high-field galvanomagnetic properties and the Fermi surface of copper, *Phys. Rev.* **141**, 592 (1966).
- [41] M. Huberman and A. W. Overhauser, Open-orbit magnetoresistance spectra of potassium, *Phys. Rev. B* **25**, 2211 (1982).
- [42] W. Gao, N. Hao, F.-W. Zheng, W. Ning, M. Wu, X. Zhu, G. Zheng, J. Zhang, J. Lu, H. Zhang, C. Xi, J. Yang, H. Du, P. Zhang, Y. Zhang, and M. Tian, Extremely Large Magnetoresistance in a Topological Semimetal Candidate Pyrite  $\text{PtBi}_2$ , *Phys. Rev. Lett.* **118**, 256601 (2017).
- [43] A. G. Lebed and P. Bak, Theory of Unusual Anisotropy of Magnetoresistance in Organic Superconductors, *Phys. Rev. Lett.* **63**, 1315 (1989).
- [44] P. Dhakal, H. Yoshino, J. I. Oh, K. Kikuchi, and M. J. Naughton, Observation and Simulation of All Angular Magnetoresistance Oscillation Effects in the Quasi-One-Dimensional Organic Conductor  $(\text{DMET})_2\text{I}_3$ , *Phys. Rev. Lett.* **105**, 067201 (2010).
- [45] A. G. Lebed, N. N. Bagmet, and M. J. Naughton, Magic Angle Effects and Angular Magnetoresistance Oscillations as Dimensional Crossovers, *Phys. Rev. Lett.* **93**, 157006 (2004).
- [46] G. M. Danner, W. Kang, and P. M. Chaikin, Measuring the Fermi Surface of Quasi-One-Dimensional Metals, *Phys. Rev. Lett.* **72**, 3714 (1994).
- [47] T. Osada and E. Ohmichi, Magnetotransport and magnetic-field-induced density waves in low-dimensional layered conductors, *J. Phys. Soc. Jpn.* **75**, 051006 (2006).
- [48] B. Bradlyn, J. Cano, Z. Wang, M. G. Vergniory, C. Felser, R. J. Cava, and B. A. Bernevig, Beyond Dirac and Weyl fermions: Unconventional quasiparticles in conventional crystals, *Science* **353**, aaf5037 (2016).
- [49] G. Chang, S.-Y. Xu, S.-M. Huang, D. S. Sanchez, C.-H. Hsu, G. Bian, Z.-M. Yu, I. Belopolski, N. Alidoust, H. Zheng, T.-R. Chang, H.-T. Jeng, S. A. Yang, T. Neupert, H. Lin, and M. Z. Hasan, Nexus fermions in topological symmorphic crystalline metals, *Sci. Rep.* **7**, 1688 (2017).
- [50] A. Ramires and J. L. Lado, Impurity-induced triple point fermions in twisted bilayer graphene, *Phys. Rev. B* **99**, 245118 (2019).